J. Fluid Mech. (2011), *vol.* 674, *pp.* 227–243.
doi:10.1017/S0022112011000103

The rapid advance and slow retreat of a mushy zone

NICHOLAS R. GEWECKE† AND TIM P. SCHULZE

Department of Mathematics, University of Tennessee, Knoxville, TN 37996-0614, USA

(Received 3 June 2010; revised 22 October 2010; accepted 23 December 2010; first published online 25 March 2011)

We discuss a model for the evolution of a mushy zone which forms during the solidification of a binary alloy cooled from below in a tank with finite height. Our focus is on behaviours of the system that do not appear when either a semi-infinite domain or negligible solute diffusion is assumed. The problem is simplified through an assumption of negligible latent heat, and we develop a numerical scheme that will permit insights that are critical for developing a more general procedure. We demonstrate that a mushy zone initially grows rapidly, then slows down and eventually retreats slowly. The mushy zone vanishes after a long time, as it is overtaken by a slowly growing solid region at the base of the tank.

Key words: solidification/melting

1. Introduction

A mushy zone is a region of intermixed liquid and solid which often results from instability caused by the build-up of solute during the solidification of multi-species materials. In this paper, we focus specifically on mushy zones which occur during the solidification of a binary alloy. In a typical experiment, a tank of uniformly mixed solution is placed onto a cold boundary, inducing the growth of a thin solid layer capped by an initially expanding mushy zone. At early times, the mushy zone grows much faster than the growth of the solid layer. Later, the growth slows as the solution is largely depleted of the material which forms the dendrites. A schematic of the physical system is given in figure 1.

We aim to relax two common assumptions that have previously been applied to ease the analysis of mushy zones. The first is to assume a semi-infinite domain and apply the method of similarity solutions. This approach was used to study mushy zones which occur during solidification of binary alloys by Worster (1986) and for the case of ternary alloys by Anderson (2003). The second assumption is to assume negligible solute diffusivity. This was used by Worster (1991) to analyse convection within a mushy layer. A collection of results for solidification of binary alloys on a semi-infinite domain, notably linear and nonlinear convective instabilities, can be found in Worster (1997). Schulze & Worster (1999) and Schulze & Worster (2005) characterized boundary conditions needed at mush–liquid interfaces in the absence of solute diffusion.

While each of these assumptions is useful, they obscure some details that are otherwise present. The application of similarity solutions to the case of a semi-infinite

† Email address for correspondence: gewecke@math.utk.edu

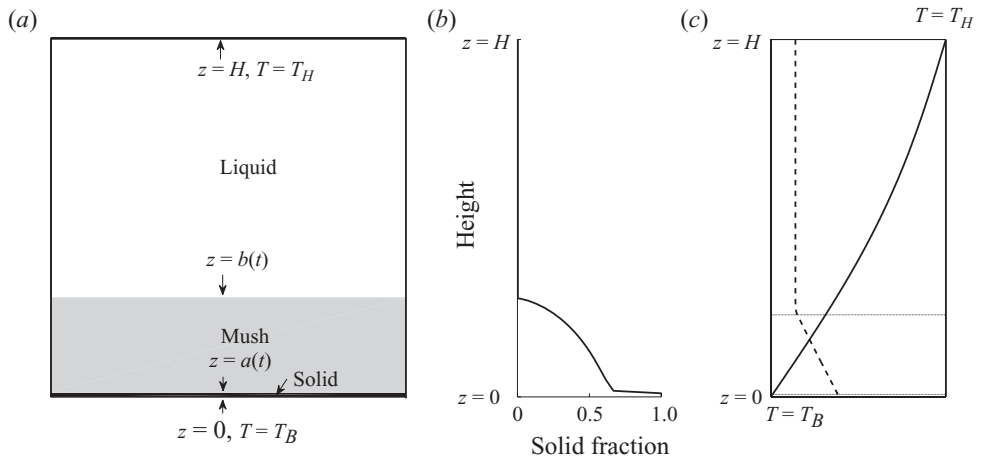

FIGURE 1. A finite-depth tank filled with a uniformly mixed solution is placed on a cold boundary. Two time-dependent interfaces form, separating the domain into three regions as shown in (*a*): a thin solid layer at the bottom (not visible on the scale shown), mush in the middle (grey), and liquid at the top (white). In (*b*), we see the corresponding curve for the solid fraction, which decreases from the solid–mush interface to the mush–liquid interface. In (*c*), representative temperature (solid, varying from $T = T_B$ to $T = T_H$) and concentration (dashed) curves are shown, with interface positions shown as horizontal lines.

domain permits the mush–liquid interface to advance like $t^{1/2}$ forever. However, the front eventually stalls out in a finite tank, since all isotherms stall out as the temperature evolves to a linear profile. The assumption of negligible solute diffusivity in a finite tank captures this effect, but the long-term behaviour of the system changes significantly compared to the system including solute diffusivity. If the temperature at the bottom of the tank is in an appropriate range, the steady-state solution with no solute diffusion involves a mushy layer and a liquid layer, whereas the steady-state solution with solute diffusion involves a solid layer and a liquid layer with no mushy layer.

Mushy zones arise in a variety of physical processes, such as the solidification of sea ice and cooling in magma chambers. In each of these cases, the spatial and temporal scales are very large in comparison to those encountered in a laboratory setting. However, the spatial domain for these processes is still finite, so behaviours exhibited by a finite-domain solution could have consequences for these applications.

The full model presents a number of challenges numerically. First, there are two free interfaces to identify. Second, the equations in the mushy layer are coupled through a latent heat term. Third, the equation governing the liquid fraction is a first-order partial differential equation. The numerical solution of such equations typically requires an upwinding scheme, which propagates data in a certain direction, and the stability of the method requires the direction to be chosen correctly.

An assumption of negligible latent heat greatly simplifies these issues, as we will discuss more thoroughly. This assumption has commonly been used in the study of mushy zones. For example, it is part of the frozen temperature approximation, which is often understood to be a collection of three assumptions (see Davis 2001): thermal diffusion is much faster than solute diffusion; latent heat is negligible; and the temperature profile is given by its steady state. The frozen temperature approximation was used by Langer (1980) to study mushy layers appearing during

directional solidification of alloys. Studies often show that the influence of latent heat is rather weak. For example, Kerr *et al.* (1990) investigated the effects of varying the Stefan number, which is equivalent to varying latent heat, when solidifying an alloy from above. The case of negligible latent heat (zero Stefan number) was included in that study. The most visible effect of increasing the Stefan number is that solidification is slowed.

In this paper, we first discuss the non-dimensional model, along with the changes resulting from the assumption of negligible latent heat. We then discuss the application of the method of characteristics to our model. Next, we generate results using our model which demonstrate that the growth of the mushy layer occurs over finite time, after which the mushy layer slowly decays until the solid–mush front overtakes the mush–liquid front. We conclude with a discussion of the results, particularly the new features which are exhibited.

2. Model

The model is based on Worster (1986) with modifications due to the finite domain. This approach treats the mushy layer as a third phase, with homogenized properties that depend upon the liquid fraction. Heat and solute are conserved locally within the mushy layer, on a scale that is larger than the pore size of the mush. The transport of heat and solute is assumed to be by diffusion alone. We will assume that the thermal properties are equal in all phases and that there is complete solute rejection. Let T denote the temperature, C denote the concentration of solute in the liquid phase and χ denote the liquid fraction in the mushy region. We non-dimensionalize the system through the scalings

$$\theta = \frac{T - T_B}{T_H - T_B}, \qquad \hat{t} = \frac{\kappa}{H^2} t, \qquad \hat{z} = \frac{1}{H} z, \tag{2.1}$$

where T_H and T_B are the respective temperatures at the top and bottom of the tank, H is the height of the tank and κ is the thermal diffusivity. We scale the concentration C and liquid fraction χ so that they range from 0 to 1. We will present non-dimensional parameters as they arise. The 'hats' on t and z will be omitted for the remainder of this paper, so any references to these two variables refer to the non-dimensional variables unless otherwise indicated. The eutectic temperature, T_E, describes the temperature at which, regardless of concentration, both components of the alloy solidify. For this problem, we require that $T_E \leqslant T_B < T_L(C_0) < T_H$, where

$$T_L(C_0) = T_M - \Gamma C_0 \tag{2.2}$$

is a model of the liquidus relationship. Here, T_M is the melting temperature of the pure material, Γ is the slope of the liquidus curve and C_0 is the initial concentration throughout the melt.

At the top of the tank, $z = 1$, we impose the conditions

$$\theta = 1 \tag{2.3a}$$

and

$$\frac{\partial C}{\partial z} = 0. \tag{2.3b}$$

These conditions describe a fixed temperature and no solute flux at the top of the tank. The condition of no solute flux is required to conserve the total amount of solute in the tank.

In the liquid region, $b(t) < z < 1$, the governing equations are

$$\frac{\partial \theta}{\partial t} = \frac{\partial^2 \theta}{\partial z^2} \tag{2.4a}$$

and

$$\frac{\partial C}{\partial t} = \epsilon \frac{\partial^2 C}{\partial z^2}, \tag{2.4b}$$

where $\epsilon = D/\kappa$ is the inverse Lewis number and D is the solute diffusivity in the dimensional model.

The interface conditions at the mush–liquid interface, $z = b(t)$, are

$$\mathscr{S}(1 - (\chi)_{b^-})\,\dot{b} = \left(\frac{\partial \theta}{\partial z}\right)_{b^-} - \left(\frac{\partial \theta}{\partial z}\right)_{b^+}, \tag{2.5a}$$

$$(C)_{b^-}\left(1 - (\chi)_{b^-}\right)\dot{b} = \epsilon(\chi)_{b^-}\left(\frac{\partial C}{\partial z}\right)_{b^-} - \epsilon\left(\frac{\partial C}{\partial z}\right)_{b^+}, \tag{2.5b}$$

$$[C]^+_- = 0, \tag{2.5c}$$

$$[\theta]^+_- = 0, \tag{2.5d}$$

where $[\cdot]^+_-$ denotes the jump of the indicated quantity across the interface, $\mathscr{S} = L/c_p \Delta T$ is the Stefan number, L denotes the latent heat, c_p denotes the specific heat and $\Delta T = T_H - T_B$. The first condition is a Stefan condition describing the balance of heat flux away from the interface with the production of latent heat. The second condition similarly balances the flux of solute away from the interface with the rejection of solute from the solid phase. The third and fourth conditions impose continuity of the concentration and temperature fields across the interface.

There is an additional condition at the mush–liquid interface, which we will discuss more thoroughly in the next section. The condition can be written as

$$\chi(b^-(t), t) = 1, \tag{2.6a}$$

when

$$\dot{b}(t) > \dot{\zeta}_b(t), \tag{2.6b}$$

where

$$\dot{\zeta}_b(t) = -\epsilon\left(\frac{\partial C}{\partial z}(b^-(t), t)\right) / C(b^-(t), t), \tag{2.7}$$

describes the propagation of the leading characteristic, as will be discussed in the next section. This condition on $\dot{b}$ refers to whether the interface is advancing more quickly than the leading characteristic, in which case $\chi = 1$ at the interface, or not, in which case the value of χ at the mush–liquid interface is given by the value along a characteristic that is terminating along the interface. We point out that the condition $\chi_b = 1$ is a special case, due to the assumption of uniform thermal properties, of the more general condition of marginal equilibrium as proposed by Worster (1986). The condition of marginal equilibrium reflects the concept that the mushy layer grows to resolve undercooling. If there is no undercooling to relieve, then this condition should not be expected to hold, but instead the mush–liquid interface will be controlled by the diffusion of solute from the mushy layer into the liquid layer.

In the mushy region, $a(t) < z < b(t)$, the governing equations are

$$\frac{\partial \theta}{\partial t} = \frac{\partial^2 \theta}{\partial z^2} - \mathscr{S}\frac{\partial \chi}{\partial t}, \tag{2.8a}$$

$$\frac{\partial (\chi C)}{\partial t} = \epsilon \frac{\partial}{\partial z}\left(\chi \frac{\partial C}{\partial z}\right), \tag{2.8b}$$

$$\theta = -\hat{\Gamma}(C - C_B), \tag{2.8c}$$

where $\hat{\Gamma} = \Gamma/(T_H - T_B)$. Additionally, C_B is the concentration along the liquidus curve corresponding to T_B, specifically $C_B = (T_M - T_B)/\Gamma$. Equation (2.8*c*) reflects the assumption of local thermal equilibrium. The rationale behind this condition is described in Worster (1986), but the main idea is that the dendrites, which constitute the solid portion of the mush, grow or melt sufficiently to maintain equilibrium. The liquidus relationship also applies at the solid–liquid interface in the absence of a mushy zone.

The interface conditions at the solid–mush interface, $z = a(t)$, are

$$\mathscr{S}(\chi)_{a^+}\dot{a} = \left(\frac{\partial \theta}{\partial z}\right)_{a^-} - \left(\frac{\partial \theta}{\partial z}\right)_{a^+}, \tag{2.9a}$$

$$(C)_{a^+}(\chi)_{a^+}\dot{a} = -\epsilon(\chi)_{a^+}\left(\frac{\partial C}{\partial z}\right)_{a^+}, \tag{2.9b}$$

$$[\theta]^+_- = 0. \tag{2.9c}$$

The first condition is a Stefan condition for jump in temperature gradient across the interface. The second condition is a similar condition describing the jump in concentration gradient; note that $C_s = 0$ due to the assumption of total solute rejection, and we assume that there is no solute diffusion within the solid phase, so there is no term representing the concentration gradient from below in this equation. The third condition imposes continuity of temperature across the interface.

The governing equation in the solid, $0 < z < a(t)$, is

$$\frac{\partial \theta}{\partial t} = \frac{\partial^2 \theta}{\partial z^2}. \tag{2.10}$$

The solid is pure, so no solute appears in this region.

The boundary condition at the bottom of the tank, $z = 0$, is

$$\theta = 0. \tag{2.11}$$

Since the temperature and concentration in the mush are coupled through (2.8*c*), we treat (2.5*b*) and (2.9*b*) as the free-boundary conditions for the mush–liquid and solid–mush interfaces, respectively.

At $t = 0$, only liquid is present, and

$$\theta(z, 0) = 1, \tag{2.12a}$$

$$C(z, 0) = C_0, \tag{2.12b}$$

for all $0 \leqslant z \leqslant 1$. These conditions reflect the uniform temperature and concentration in the tank at the beginning of an experiment.

For the rest of this paper, we will assume negligible latent heat. This simplifies the system, as the temperature equations decouple from the rest of the system. Additionally, this assumption allows the application of the method of characteristics within the mushy layer, which will be described in the next section. Thus, $L=0$ and so $\mathscr{S}=0$. Inside the mush, this changes (2.8a) to

$$\frac{\partial\theta}{\partial t}=\frac{\partial^2\theta}{\partial z^2}. \tag{2.13}$$

Also, (2.5a) and (2.9a) become

$$0=\left(\frac{\partial\theta}{\partial z}\right)_{b^-}-\left(\frac{\partial\theta}{\partial z}\right)_{b^+} \tag{2.14a}$$

and

$$0=\left(\frac{\partial\theta}{\partial z}\right)_{a^-}-\left(\frac{\partial\theta}{\partial z}\right)_{a^+}. \tag{2.14b}$$

As a result, the temperature field has no dependence upon the interface positions and no dependence upon any other quantities within the mush, so it is governed by the heat equation on the whole domain.

3. Method of characteristics

We now restrict our focus to (2.8b), so that we can motivate part of our numerical procedure and explain the condition given by (2.6a) and (2.6b). Equation (2.8b) can be rewritten as

$$\frac{\partial\chi}{\partial t}-\frac{\epsilon}{C}\left(\frac{\partial C}{\partial z}\right)\left(\frac{\partial\chi}{\partial z}\right)+\frac{1}{C}\left(\frac{\partial C}{\partial t}\right)\chi-\frac{\epsilon}{C}\left(\frac{\partial^2 C}{\partial z^2}\right)\chi=0. \tag{3.1}$$

Due to the liquidus constraint given by (2.8c) and the fact that the temperature is the solution of the heat equation, this equation is a first-order partial differential equation governing the liquid fraction χ. As such, the method of characteristics can be applied to solve this equation. Applying this method, as can be found in Evans (1998) as well as other sources, we find that the characteristics satisfy

$$\dot{\zeta}(s)=\left(\frac{-\epsilon}{C(\zeta(s),\tau(s))}\right)\frac{\partial C}{\partial z}(\zeta(s),\tau(s)), \tag{3.2a}$$

$$\dot{\tau}(s)=1, \tag{3.2b}$$

$$\dot{\chi}(s)=\frac{1}{C(\zeta(s),\tau(s))}\left(\epsilon\frac{\partial^2 C}{\partial z^2}(\zeta(s),\tau(s))-\frac{\partial C}{\partial t}(\zeta(s),\tau(s))\right)\chi(s), \tag{3.2c}$$

where ζ and τ correspond to spatial position and time. Equation (3.2b) indicates that if a characteristic curve is initiated at some point (z_0,t_0) then $\tau=s+t_0$, so τ and t correspond directly with each other. Additionally, (3.2c) can be integrated in s to find

$$\chi(s)=\chi(0)\exp\left(\int_0^s\frac{\epsilon\dfrac{\partial^2 C}{\partial z^2}(\zeta(\xi),\tau(\xi))-\dfrac{\partial C}{\partial t}(\zeta(\xi),\tau(\xi))}{C(\zeta(\xi),\tau(\xi))}\,\mathrm{d}\xi\right). \tag{3.3}$$

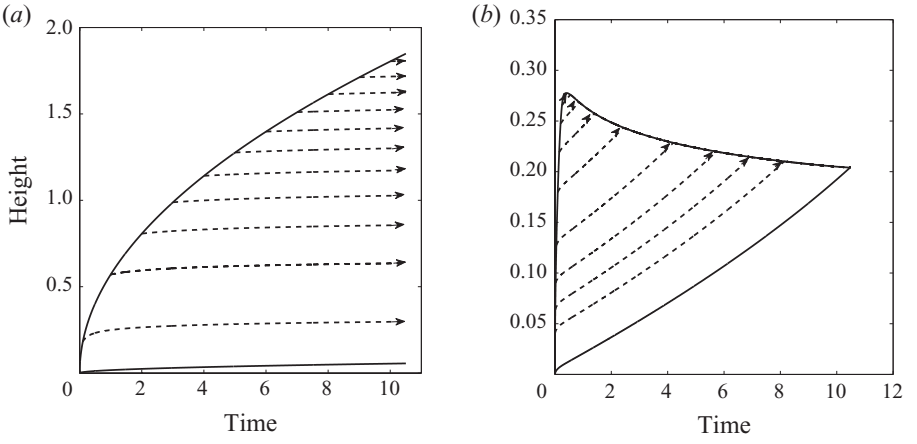

FIGURE 2. In both images, the characteristics are given by dashed curves. The solid curves denote the solid–mush interface (lower curve) and the mush–liquid interface (upper curve). The infinite-domain case is shown in (*a*) and the finite-domain case is shown in (*b*).

The temperature field satisfies $\theta_z > 0$ for all $0 \leqslant z \leqslant 1$ and for all $t > 0$. By the liquidus relationship, we then have $C_z < 0$ throughout the mush. Additionally, $C > 0$ holds throughout the mush. As a result, we see from (3.2*a*) that the characteristic curves will always advance. That is, $\dot{\zeta}(s) > 0$ for all $s > 0$.

Taking the above into account, we can address the boundary condition for χ given by (2.6*a*). In Worster (1986), a condition of marginal equilibrium was enforced at the mush–liquid interface. Under the assumption of uniform thermal properties, this implies $\chi_b = 1$. This condition was appropriate because the interface was always advancing at a sufficiently high rate, proportional to $t^{-1/2}$. In the present case, the interface cannot advance at that rate for all time since this would eventually force concentration values in the mush to become negative. More specifically, since the solute is completely rejected from the solid phase, the mush–liquid interface cannot advance beyond the isotherm corresponding to $\theta_L(C_0)$.

Examination of the characteristics can further illuminate this situation. As illustrated in figure 2(*a*), for the infinite-domain problem the characteristic curves emerge from the mush–liquid front and advance slower than the front for all time, so the characteristic curves never intersect with the front after they emerge. In the case of a finite domain, the maximum height of the mush is restricted due to the temperature and concentration profiles and will always be below the upper boundary. If we assume that the temperature field has reached its steady state and that a mushy region is still present, then the characteristics advance at a rate that is bounded below, since $0 < C \leqslant C_E$ and

$$\dot{\zeta}(s) = \frac{-\epsilon \dfrac{\partial C}{\partial z}(\zeta(s), \tau(s))}{C(\zeta(s), \tau(s))},$$

$$= \frac{\epsilon}{\hat{\Gamma} C(\zeta(s), \tau(s))} \geqslant \frac{\epsilon}{\hat{\Gamma} C_E}. \tag{3.4}$$

Therefore, each characteristic curve will intersect with the mush–liquid interface in finite time. The condition $\chi_b = 1$ is inconsistent with the value of χ along those

characteristic curves. In figure 2(*b*), we see how characteristics for the finite-domain problem intersect with the mush–liquid interface.

In terms of the characteristic curves, we set $\chi_b = 1$ whenever characteristic curves are emerging from the mush–liquid interface, which occurs when the interface velocity is greater than the velocity of the leading characteristic, corresponding to the assumption of marginal equilibrium described by Worster (1986). In a more general situation, where the thermal properties in the solid and liquid could be different, the value of χ_b for emerging characteristics would be determined using the assumption of marginal equilibrium. When characteristic curves terminate along the interface, which occurs when the interface velocity is less than the velocity of the leading characteristic, χ_b is taken to be the value of χ along the terminating characteristic. This is always the case when the interface is retreating. In other words, the condition of marginal equilibrium, reflected in the condition given by (2.6*a*), is a physical principle which provides a closure condition when such a condition is needed.

The possibility that characteristics intersect with a mush–liquid interface that is advancing relative to the solid phase is noteworthy, as this does not seem to occur in situations previously considered. For example, Schulze & Worster (2005) consider boundary conditions along mush–liquid interfaces in the absence of solute diffusion, but with a solid phase that moves steadily relative to the liquid phase. In that case, and in similar crystal pulling scenarios where diffusion is neglected, the liquid fraction characteristics move with the velocity of the solid phase, so that the comparison of velocity and characteristic velocity can be simply characterized in terms of an interface that is expanding or retreating with respect to the solid phase. However, in the presence of solute diffusion, the characterization changes to that discussed above.

An important result that simplifies the problem is that the solid–mush interface follows a characteristic. It can be shown, see the Appendix, that $\chi_a = 0$ for the similarity solution with no latent heat. Clearly, $\chi_a = 0$ is a solution for the free-boundary condition given by (2.9*b*). A characteristic initialized with $\chi(0) = 0$ would maintain $\chi(s) = 0$ due to (3.3). Therefore, such a characteristic would satisfy the interface condition. However, if the interface advanced more rapidly than this characteristic, then the liquid fraction at the solid–mush interface would be determined by a characteristic terminating on the interface, so $\chi_a \neq 0$, and (2.9*b*) becomes

$$\dot{a} = \frac{-\epsilon}{(C)_{a^+}} \left(\frac{\partial C}{\partial z} \right)_{a^+}, \tag{3.5}$$

which is (3.2*a*) applied at $z = a$. This indicates that the interface advance is the same as the advance of a characteristic, which would contradict the assumption that the interface was advancing more rapidly than a characteristic. Therefore, the solid–mush interface always satisfies $\chi_a = 0$ and it travels along a characteristic. Since all characteristics eventually intersect the mush–liquid interface in finite time, we conclude that the solid–mush interface will do the same. This implies that the mush will completely disappear in finite time.

4. Steady states

An important difference between the cases where solute diffusion is present and where it is absent appears in the associated steady states. In the case $\epsilon = 0$, where

solute diffusion is assumed to be negligible, the steady state is given by

$$\left.\begin{aligned} \theta(z) &= z, \\ C(z) &= \begin{cases} C_0, & \hat{\Gamma}(C_B - C_0) \leqslant z \leqslant 1, \\ \dfrac{\hat{\Gamma} C_B - z}{\hat{\Gamma}}, & 0 \leqslant z \leqslant \hat{\Gamma}(C_B - C_0) \end{cases} \\ \chi(z) &= \begin{cases} 1, & \hat{\Gamma}(C_B - C_0) \leqslant z \leqslant 1, \\ \dfrac{\hat{\Gamma} C_0}{\hat{\Gamma} C_B - z}, & 0 \leqslant z \leqslant \hat{\Gamma}(C_B - C_0). \end{cases} \end{aligned}\right\} \tag{4.1}$$

Note that this steady state does not include a solid region.

In the case $\epsilon > 0$, where solute diffusion is present, the steady state is given by

$$\left.\begin{aligned} \theta(z) &= z, \\ C(z) &= \begin{cases} 0, & 0 \leqslant z < h^* \\ \dfrac{C_0}{1 - h^*}, & h^* \leqslant z \leqslant 1, \end{cases} \\ \chi(z) &= \begin{cases} 0, & 0 \leqslant z < h^* \\ 1, & h^* \leqslant z \leqslant 1, \end{cases} \end{aligned}\right\} \tag{4.2}$$

$$h^* = \tfrac{1}{2}\left(1 + \hat{\Gamma} C_B - \sqrt{(1 - \hat{\Gamma} C_B)^2 + 4\hat{\Gamma} C_0}\right). \tag{4.3}$$

Note that this steady state does not include a mushy region. Instead, there is a solid region in equilibrium with a liquid region of increased concentration.

From the above, we see that the assumption of negligible solute diffusion results in a steady-state mushy zone, but the presence of diffusion eliminates that mushy zone and results in a phase-separated steady state.

5. Numerical method

The full model with non-zero latent heat poses many challenges numerically. At each time step, the positions of the two free interfaces must be determined. The coupled partial differential equations in the mush require careful consideration. In addition, calculations of the solutions of the differential equations in each of the three regions depend upon the interface locations, which themselves depend upon the solutions of the differential equations. Accurately solving for the liquid fraction requires the solution of a first-order partial differential equation, which requires upwinding to be performed in the correct direction.

The assumption of negligible latent heat alleviates a number of these challenges. The key benefit is that the temperature field no longer depends upon the liquid fraction in the mush, but is instead governed by the heat equation over the whole domain. This allows the temperature field to be calculated separately from all other quantities in the problem. Applying the method of characteristics allows us to track the liquid fraction using a simple formula, and it allows us to track the solid–mush interface position without any additional effort since this interface follows a characteristic. Once the temperature field has been calculated, we utilize the liquidus relationship to determine the concentration values in the mush. This leaves two quantities whose

numerical solutions rely heavily on each other: concentration in the liquid region and the mush–liquid interface position.

While the numerical procedure utilized here will not directly translate to the non-zero latent heat case, the intent is to generate a comparatively simple procedure to gain insight into various behaviours of the system. These insights can then inform future construction of a numerical procedure which will include the latent heat terms. We first present the various spatial discretizations used and proceed with a description of the numerical scheme.

5.1. *Discretization*

The discretizations of the various quantities in this problem are handled in different ways. Essentially, the simplest discretizations that worked well were utilized.

For liquid fraction within the mush, we do not utilize a spatially uniform discretization. Instead, we track the characteristics within the mush. The temperature field is tracked independently of the characteristics, which allows for this choice.

A spatially uniform mesh over the entire domain is utilized for the temperature field. The interface positions do not influence the temperature field at all, so splitting the domain for the temperature field into three pieces would introduce unnecessary complications. Since we use characteristics to track the liquid fraction in the mush, additional work is required to incorporate data for the concentration in the mush to solve the characteristic equations, where the concentration in the mush is determined by the liquidus relationship. Either a non-uniform mesh or interpolation is required. We utilize interpolation since interpolating the data seems the better approach and solving for the temperature field on the whole domain is easier than solving on three domains.

The concentration only needs to be solved for in the liquid region. For this, we use a spatially uniform mesh in the liquid. This domain is dependent upon time, so the mesh varies with time. To handle this, we map the liquid region $(b(t), 1)$ to the fixed domain $(0, 1)$. Specifically, the transformation is given by

$$\tau = t, \quad \xi = \frac{z - b(t)}{1 - b(t)}. \tag{5.1}$$

This transformation changes (2.4*b*) into

$$\frac{\partial C}{\partial \tau} - \frac{(1-\xi)\dot{b}(\tau)}{H - b(\tau)} \frac{\partial C}{\partial \xi} = \frac{\epsilon}{(H - b(\tau))^2} \frac{\partial^2 C}{\partial \xi^2}. \tag{5.2}$$

The gridpoints in $(0, 1)$ do not move, so data at the previous time step can be utilized directly. This transformation introduces a first-order spatial derivative which accounts for the movement of the gridpoints in the original variables.

5.2. *Scheme*

We initialize the system at some very small initial time t_s using the similarity solution from Worster (1986). A small number of characteristics are initiated at this time, including a characteristic at each of the two interfaces. In line with the fact that the liquid fraction along the solid–mush interface is zero, see the Appendix, the corresponding characteristic is initiated with $\chi = 0$.

For each following time step t_i, we do the following.

(i) We update the temperature distribution over the whole domain.

(ii) For each characteristic present at t_{i-1}, we update the position and liquid fraction data, assuming that all characteristics remain in the mush. The values for

concentration and its derivatives are calculated using the liquidus relationship and interpolating the values of θ and its derivatives. Since the solid–mush interface follows a characteristic, this procedure updates that interface position a_i.

(iii) We then determine the location of the mush–liquid interface b_i:

(a) We guess an interface position b_i and a secondary guess $b_i + \delta$, with δ small.

(b) The concentration field in the liquid is calculated using the two guess values above.

(c) Residuals for each of the two guesses are calculated using (2.5b). For each guess, the liquid fraction at the mush–liquid interface is set to unity if the guess is ahead of the leading characteristic or to an interpolated value if the guess is behind the leading characteristic. Specifically, we determine the two characteristics bounding the guess, then interpolate the liquid fraction values between those characteristics.

(d) Using the residuals calculated in the previous step, we use a secant-line approximation of the derivative in a Newton iteration to update the guess for b_i. With this updated guess, we repeat the previous two steps.

(e) Once the size of the change for the guess is small enough, we terminate the iteration. If the accepted value of b_i is ahead of the leading characteristic, we initialize a characteristic at (b_i, t_i) with $\chi = 1$. If the accepted value of b_i is not ahead of the leading characteristic, we remove characteristics as needed so that the leading characteristic is at (t_i, b_i). In practice, we remove characteristics by setting their positions at t_i to be b_i and by setting their liquid fraction values to the value determined for the interface position. We then proceed to the next time step.

6. Results

In order to connect with potential future experiments, we will be presenting many of our results in terms of the unscaled variables. All graphs will be in terms of the scaled variables. The parameters used to generate our results are taken from Set I of table 1 in Worster (1986), which are a reasonable approximation to the values in the corresponding Set II addressing the assumption of uniform thermal properties, with modifications for our treatment of the concentration as a fraction rather than a percentage. These parameters roughly approximate a 14 % sodium nitrate solution. The initial temperature of the tank T_H is taken to be 15°C, and the temperature of the cold surface T_B is taken to be −15.6°C. Additionally, the tank has a height of 15 cm. These parameters correspond to the non-dimensional values $\epsilon \approx 7.7 \times 10^{-3}$, $\hat{\Gamma} \approx 1.307$ and $C_B = 0.39$, and the melting temperature of the pure material $T_M = 0$ corresponds to $\theta \approx 0.51$.

The interface positions through time are shown in figure 3. For the parameters used, the time for the mush–liquid interface to reach its maximum height of approximately 4 cm is approximately one day. In that time, the solid–mush interface has only reached a height of approximately 0.25 cm. The mush–liquid interface then begins to retreat slowly and the solid–mush interface continues a steady advance. After approximately 22 days the mush vanishes. During the retreat of the mush–liquid interface, the liquid fraction at the interface decreases. After the mush vanishes, the solid–liquid interface is shown; see Worster (1986) for the appropriate interface conditions.

In figure 4, we can see how the liquid fraction varies as time progresses. As long as a particular spatial point stays in the mush, the liquid fraction at that point decreases

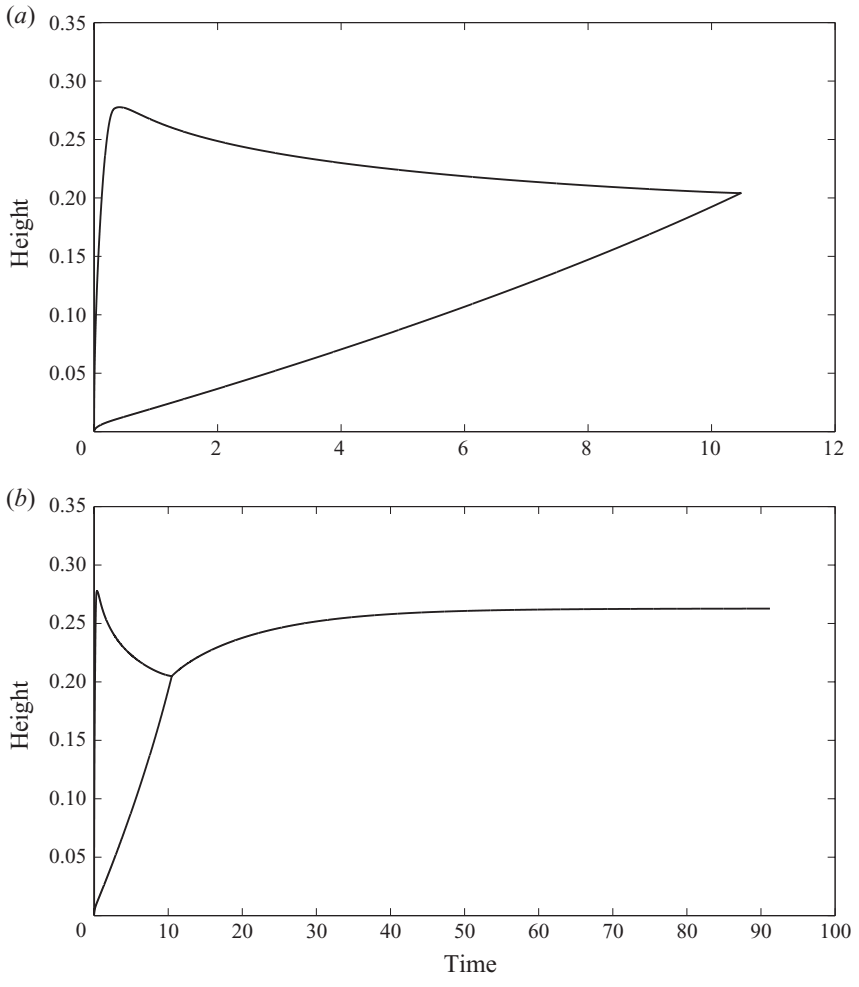

FIGURE 3. In (*a*), the solid–mush (lower curve) and mush–liquid (upper curve) interface positions are shown from $t = 0$ to the time when the mush vanishes. The long-time behaviour is shown in (*b*), with only a single curve denoting the solid–liquid interface once the mush has vanished. The parameters used are provided in the main text.

with time. In figure 5, we can see how the temperature profile changes. This should be recognized as the solution of the heat equation on a finite domain. In figure 6, we can see how the concentration profile varies in the liquid. The final concentration curve shown relates to the time when the mush vanishes.

In figure 7, the solution during the early times is compared with the similarity solution from Worster (1986). The curves match up very well for a significant portion of the time until the mush–liquid interface reaches its maximum height. The curve for the mush–liquid interface in the similarity solution eventually outpaces the finite-domain solution, but this is expected due to the similarity solution having no bound on how far it could advance. The solid–mush interface is well approximated by the similarity solution over the interval shown, but it too will eventually stop advancing in the finite tank.

In figure 8, the solution for the mush–liquid interface during the early times is compared with the solution for $\epsilon = 0$ on a finite domain. The curves match up fairly

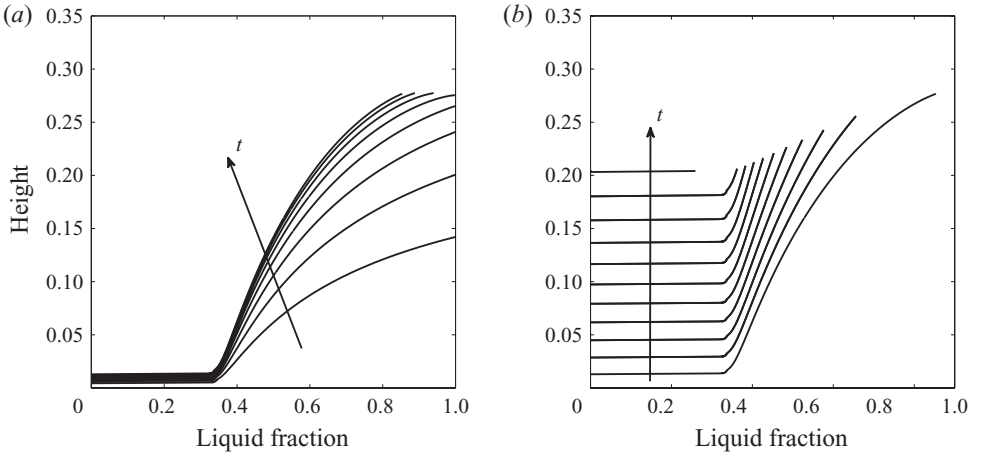

FIGURE 4. The curves are liquid fraction (χ) profiles within the mush at various stages of system evolution. The curves in (a) are at evenly-spaced intervals during the advance of the mush–liquid interface. The remainder of the time until the mush vanishes is illustrated in (b), again at evenly-spaced intervals.

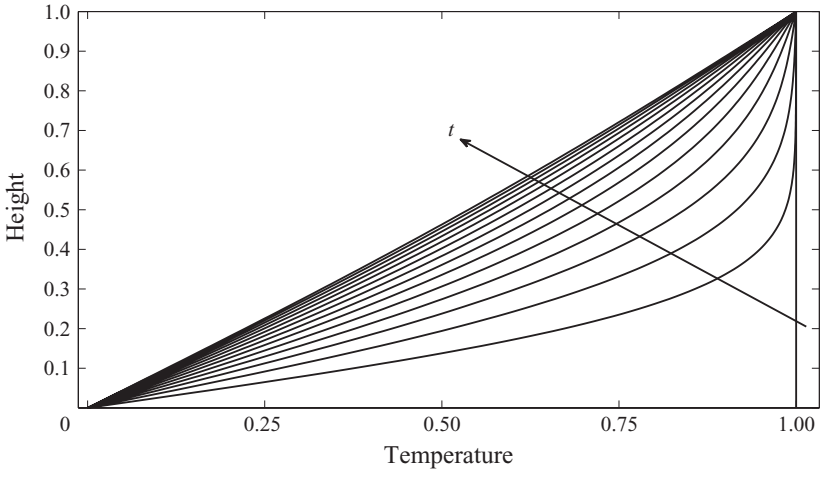

FIGURE 5. The curves shown are temperature profiles at regular intervals over the time scale for thermal diffusivity. Time progresses in the direction shown by the arrow. By the last time shown, the temperature profile is near its steady state.

well during the times shown. The advance of the mush–liquid interface position is well approximated by the $\epsilon = 0$ solution, but the $\epsilon = 0$ solution does not capture the retreat of the interface, as highlighted in figure 9. Additionally, the $\epsilon = 0$ solution does not exhibit an advancing solid–mush interface. The absence of the solid–mush front when $\epsilon = 0$ is caused by (2.8b) transforming into

$$\frac{\partial}{\partial t}(\chi C) = 0, \tag{6.1}$$

which prevents $\chi_a = 0$, so the only permissible solution of (2.9b) is $\dot{a} = 0$.

Other trials confirm that the time scales with H^2 and the heights of the fronts scale with H, as can be predicted from the scaling of the system.

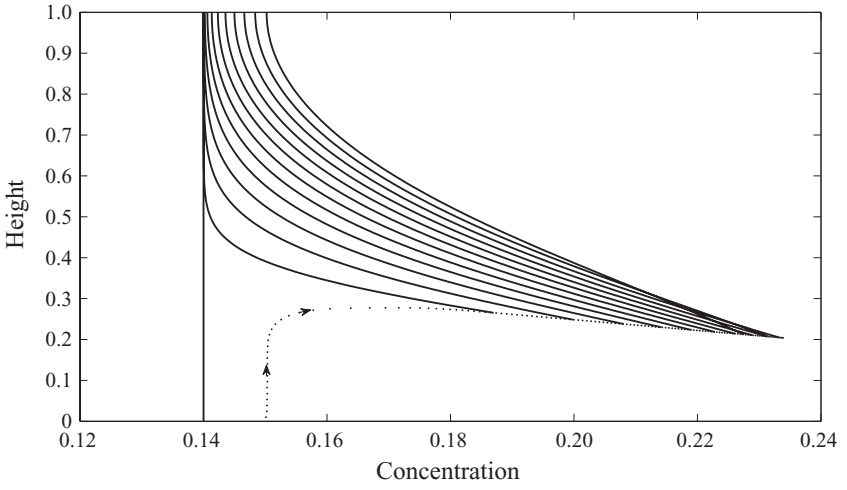

FIGURE 6. The curves shown are concentration profiles in the liquid at various stages of system evolution. The profiles shown are at evenly-spaced intervals, starting at $t = 0$. The dotted curve indicates the concentration at the mush–liquid interface. The arrows along the dotted curve indicate the direction of time progression.

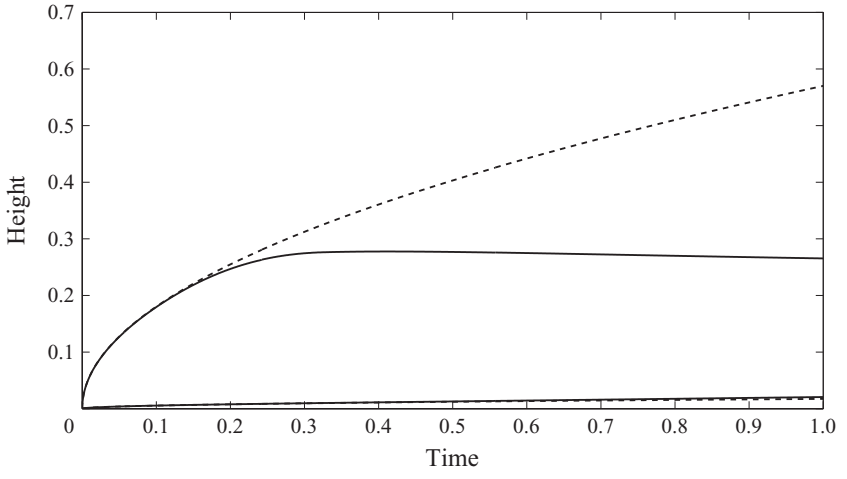

FIGURE 7. The interface positions for the finite-domain solution (solid curves) are compared with those for the infinite-domain similarity solution from Worster (1986) (dashed curves). The upper curves are the mush–liquid interfaces, and the lower curves are the solid–mush interfaces.

A boundary-layer analysis can also provide useful insights into the system. Consider expansions of the form

$$f(z,t) = f_0(z,t) + \epsilon f_1(z,t) + \epsilon^2 f_2(z,t) + \cdots \tag{6.2}$$

for the temperature, concentration and liquid fraction. To leading order, the equations governing the temperature distribution do not change, but the equations governing concentration and liquid fraction change to the equations for $\epsilon = 0$. This forms the boundary layer, which corresponds to the time frame of the rapid advance of the mush–liquid front and has (4.1) as its steady state.

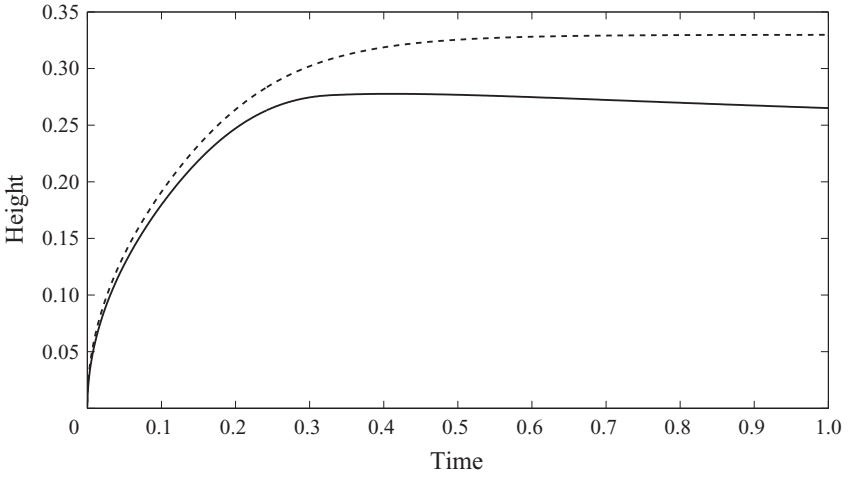

FIGURE 8. The mush–liquid interface position for early times (solid curve) is compared with the same interface for the $\epsilon = 0$ solution (dashed curve).

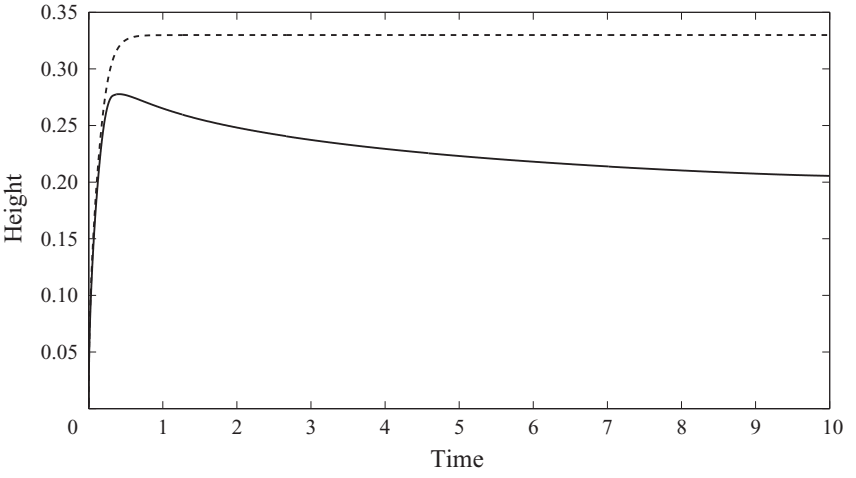

FIGURE 9. The mush–liquid interface (solid curve) for large times is compared with the corresponding interface in the $\epsilon = 0$ solution (dashed curve).

For a rescaling to large time, specifically $t \to \epsilon^{-1}t$, most of the equations change. Specifically, the temperature profile becomes fixed, as the continuity of temperature and its gradients continues to hold at each interface, but in each of the three regions,

$$\frac{\partial^2 \theta}{\partial z^2} = 0. \tag{6.3}$$

Thus, the long-time solution has $\theta = z$. The concentration and liquid fraction equations transform to the equations in the system with $\epsilon = 1$. This long-time solution has (4.2) as its steady state.

Combining the above, the leading-order solution for early times is the $\epsilon = 0$ solution. For large time values, the temperature solution becomes fixed, and the retreat of the mush–liquid interface and the advance of the solid–mush interface come into effect.

7. Conclusions

When a finite-height tank filled with a uniformly mixed binary alloy is placed onto a cooled boundary, a mushy zone initially advances rapidly from that boundary. As time passes, this advance stops. Eventually, the mush–liquid interface begins to retreat very slowly. There is also a pure solid layer that grows slowly. After a sufficiently large amount of time, the solid–mush interface catches up to the mush–liquid interface, eliminating the mushy layer. After this occurs, the system continues to solidify without a mushy layer until the liquid region homogenizes.

The assumption of negligible latent heat was critical in this analysis, permitting the use of the method of characteristics. A similar numerical approach to the one presented may be applicable in the presence of latent heat. Such an approach would iterate on the temperature field and both the position of and liquid fraction along characteristics at the new time step. The liquid fraction at the solid–mush interface will no longer be zero, as this particular condition is a direct result of negligible latent heat. The behaviours exhibited in the present analysis would still occur. For instance, the steady states remain unchanged when latent heat is included. Additionally, the mush–liquid interface remains bounded by the isotherm associated with $\theta_L(C_0)$ and the solid–mush interface will slowly advance until the mush vanishes. As previously discussed, varying the Stefan number slows solidification, so the mushy layer may persist longer than predicted here, but it will ultimately vanish.

Much effort has been invested in studying convective instabilities of mushy zones, as can be seen from the review in Worster (1997). The results of such investigations should still apply to the present case. For solidification from below, if the rejected component is less dense than the component making up the dendrites, then buoyancy-driven convection is anticipated. In such a case, the long-term behaviour demonstrated in this paper may be disrupted. If the rejected component has higher density, then convection is not expected.

We anticipate that a simple experimental set-up could be utilized to validate our results. Our parameters roughly approximate a 14 % sodium nitrate solution, as described in Set I of table 1 in Worster (1986), so a tank filled with such a solution at 15°C placed upon a surface cooled to −15.6°C should reflect the results we have provided. The specific results given in this paper are for a tank that has a height of 15 cm, but a smaller tank would permit such an experiment to be completed in a more reasonable amount of time due to the scaling of time with H^2. For example, a tank with height 3 cm filled with a uniformly mixed 14 % sodium nitrate solution is predicted to have no mushy zone remaining after one day.

An experimental set-up for directional solidification has recently been developed, as described in Peppin *et al.* (2007). Some experimental results obtained with this apparatus have also been described in Peppin, Huppert & Worster (2008). In particular, they show that the mushy layer grows initially, reaches a state which it maintains for some time, and eventually begins to slowly retreat. Such results would seem to highlight the distinction between the finite-size Hele–Shaw cell used in the experiment and the infinite-length domain used in analytical results. We suspect that we are demonstrating a similar issue, but in a different experimental arrangement.

In this paper, we have focused exclusively on the case where $T_B > T_E$. The purpose of this restriction was to eliminate the possibility of a eutectic front. A eutectic front would have different interface conditions from those used in this model. Specifically, the free-boundary condition becomes $T = T_E$, and (2.9*b*) is modified to determine the solid fraction due to solute being frozen into the solid region. These conditions are

given for ternary alloys in Anderson (2003) and are similar for binary alloys. We suspect that the dynamics of the system with $T_B < T_E$ will have similarities to the case we have discussed, but will exhibit some unique behaviours. In particular, if a eutectic front appears at early times, there will eventually be a switch from a eutectic solid–mush front to a solid–mush front of the type we have discussed in this paper, where $C_s = 0$. After such a switch occurs, the system will evolve in a fashion similar to what we have discussed in this paper. The steady-state solutions will be different, as some of the solute will be trapped in the eutectic solid in the bottom region of the tank.

We are grateful to M. G. Worster and D. M. Anderson for helpful discussions. We would also like to acknowledge support from the National Science Foundation, through grant numbers DMS-0405650 and DMS-0707443.

Appendix. Liquid fraction at the solid–mush interface

The appendix is available online as supplementary material at journals.cambridge.org/flm.

REFERENCES

Anderson, D. M. 2003 A model for diffusion-controlled solidification of ternary alloys in mushy layers. *J. Fluid Mech.* **483**, 165–197.

Davis, S. H. 2001 *Theory of Solidification*. Cambridge University Press.

Evans, L. C. 1998 *Partial Differential Equations*. American Mathematical Society.

Kerr, R. C., Woods, A. W., Worster, M. G. & Huppert, H. E. 1990 Solidification of an alloy cooled from above. Part 1. Equilibrium growth. *J. Fluid Mech.* **216**, 323–342.

Langer, J. S. 1980 Instabilities and pattern formation in crystal growth. *Rev. Mod. Phys.* **52**, 1–28.

Peppin, S. S. L., Aussillous, P., Huppert, H. E. & Worster, M. G. 2007 Steady-state mushy layers: experiments and theory. *J. Fluid Mech.* **570**, 69–77.

Peppin, S. S. L., Huppert, H. E. & Worster, M. G. 2008 Steady-state solidification of aqueous ammonium chloride. *J. Fluid Mech.* **599**, 465–476.

Schulze, T. P. & Worster, M. G. 1999 Weak convection, liquid inclusions and the formation of chimneys in mushy layers. *J. Fluid Mech.* **388**, 197–215.

Schulze, T. P. & Worster, M. G. 2005 A time-dependent formulation of the mushy-zone free-boundary problem. *J. Fluid Mech.* **541**, 193–202.

Worster, M. G. 1986 Solidification of an alloy from a cooled boundary. *J. Fluid Mech.* **167**, 481–501.

Worster, M. G. 1991 Natural convection in a mushy layer. *J. Fluid Mech.* **224**, 335–359.

Worster, M. G. 1997 Convection in mushy layers. *Annu. Rev. Fluid Mech.* **29**, 91–122.